Clin Orthop Relat Res (2011) 469:2915–2924
DOI 10.1007/s11999-011-1912-0

BASIC RESEARCH

Delayed Fracture Healing in Growth Differentiation Factor 5-deficient Mice

A Pilot Study

Cynthia M. Coleman PhD, Brooke H. Scheremeta DO, Amanda T. Boyce PhD, Robert L. Mauck PhD, Rocky S. Tuan PhD

Received: 26 July 2010 / Accepted: 29 April 2011 / Published online: 18 May 2011
© The Association of Bone and Joint Surgeons® 2011

Abstract

Background Growth differentiation factor-5 (GDF-5) is a key regulator of skeletogenesis and bone repair and induces bone formation in spinal fusions and nonunion applications by enhancing chondrocytic and osteocytic differentiation and stimulating angiogenesis. Elucidating the contribution of GDF-5 to fracture repair may support its clinical application in complex fractures.

Questions/purpose We therefore asked whether the absence of GDF-5 during fracture repair impaired bone healing as assessed radiographically, histologically, and mechanically.

Methods In this pilot study, we performed tibial osteotomies on 10-week-old male mice, stabilized by intramedullary and extramedullary nailing. Healing was assessed radiographically and histologically on Days 1 (n = 1 wild-type; n = 5 bp [brachopodism]), 5 (n = 3 wild-type; n = 3 bp), 10 (n = 6 wild-type; n = 3 bp), 14 (n = 6 wild-type; n = 6 bp), 21 (n = 6 wild-type; n = 6 bp), 28 (n = 7 wild-type; n = 6 bp), and 56 (n = 6 wild-type; n = 6 bp) after fracture. After 10 (n = 7 wild-type; n = 7 bp contralateral and n = 3 bp fractured tibiae), 14 (n = 6 wild-type; n = 6 bp), 21 (n = 6 wild-type; n = 6 bp), 28 (n = 6 wild-type; n = 3 bp), and 56 (n = 8 wild-type; n = 6 bp) days, the callus cross-sectional area was calculated. We characterized the mechanical integrity of the healing fracture by yield stress and Young's modulus at 28 (n = 6 wild-type; n = 3 bp) and 56 (n = 8 wild-type; n = 6 bp) days postfracture.

Results The absence of GDF-5 impaired cartilaginous matrix deposition in the callus and reduced callus cross-sectional area. After 56 days, the repaired bp fracture was mechanically comparable to that of controls.

Conclusions Although GDF-5 deficiency did not compromise long-term fracture healing, a delay in cartilage formation and remodeling supports roles for GDF-5 in the early phase of bone repair.

One or more of the authors (RT) received funding from National Institutes of Health grant ZO1 AR41131.
Each author certifies that his or her institution approved the animal protocol for this investigation and that all investigations were conducted in conformity with ethical principles of research.
This work was performed at the Cartilage Biology and Orthopaedics Branch, National Institute of Arthritis and Musculoskeletal and Skin Diseases, National Institutes of Health, Department of Health and Human Service, Bethesda, MD, USA.

C. M. Coleman, B. H. Scheremeta, A. T. Boyce, R. L. Mauck, R. S. Tuan
Cartilage Biology and Orthopaedics Branch, National Institute of Arthritis and Musculoskeletal and Skin Diseases, National Institutes of Health, Department of Health and Human Service, Bethesda, MD, USA

C. M. Coleman
Regenerative Medicine Institute, National University of Ireland Galway, Galway City, County Galway, Ireland

B. H. Scheremeta
Schneider Children's Hospital, New Hyde Park, NY, USA

R. L. Mauck
McKay Orthopaedic Research Laboratory, Department of Orthopaedic Surgery, University of Pennsylvania, Philadelphia, PA, USA

R. S. Tuan (✉)
Center for Cellular and Molecular Engineering, Department of Orthopaedic Surgery, University of Pittsburgh School of Medicine, 450 Technology Drive, Room 221, Pittsburgh, PA 15219, USA
e-mail: rst13@pitt.edu

Clinical Relevance Local delivery of GDF-5 to clinically difficult fractures may simulate cartilage formation in the callus and support subsequent remodeling.

Introduction

GDF-5 is a member of the transforming growth factor-β (TGF-β) superfamily of signaling molecules [3, 25, 31]. GDF-5 is expressed embryonically in precartilage condensations [7, 15, 43], the cartilaginous core of long bones [7, 15], on articular surfaces and joint interzones [7, 15], and along the perichondrium [7, 15]. In embryonic chondrogenesis, GDF-5 increases chondroprogenitor migration and condensation in vitro [8, 9, 15, 21] and in vivo [15, 46]. Exogenous GDF-5 induces de novo chondrogenesis [43], osteogenesis [11, 26, 29, 39, 40, 50], tenogenesis [47], and angiogenesis [48]. Supplementation of GDF-5 to mesenchymal progenitor cells in culture increases chondrogenic pellet size [2], cellular proliferation [18, 19], and stimulates the expression of chondrogenic and osteogenic markers [2, 18, 19, 28, 38, 49, 51, 52]. GDF-5 therefore is an important signaling molecule in skeletal development and thus may have therapeutic potential for the repair of these tissues.

Mutations in the human homologue of GDF-5, cartilage-derived morphogenetic protein 1, result in multiple acromesomelic chondrodysplasias, including Grebe type [1, 10, 13, 41, 45], Hunter-Thompson type [45], Du Pan [14, 24, 44], brachydactyly type C [12, 16, 33, 35], brachydactyly type A2 [27, 36], and symphalangism [36]. These syndromes present with a healthy axial skeleton and altered limb anatomy, including long bone shortening, bone fusions, and misalignment. Murine mutations in GDF-5 result in brachypodism (bp [42]), wherein the mice have shortened, more compliant long bones [32], morphologic changes in articulations of the knees and hips, loss of tendons, and fusions of skeletal elements in the paws, ankles, and wrists [20, 30, 42].

Administration of GDF-5 induces de novo bone formation at ectopic sites [11, 39, 40] in applications such as spinal fusion [26, 39, 40], nonunion repair [39, 40], and calvarial defects [29, 50]. However, GDF-5 is less osteogenic than the more commonly used members of the TGF-β family, such as OP-1 [18, 19]. As is true for several TGF-β superfamily proteins [17], the functional roles of GDF-5 in bone fracture repair involve enhancement of osteogenic differentiation [38, 49, 51, 52] and angiogenesis [37, 38, 48], thereby supporting bone regeneration. In repairing fractures, GDF-5 mRNA expression is localized to chondroid bone with considerable expression in the callus [6, 34]. The greatest expression of GDF-5 correlates with peak expression of collagen type II, suggesting a close link between GDF-5 and the chondral phase of fracture repair [6]. Chhabra et al. observed a delay in femoral fracture repair in the absence of GDF-5 protein resulting from delayed cellular recruitment and chondrogenesis in the callus [5], suggesting a similar function for GDF-5 in adult reparative situations as that in skeletogenesis [9, 15]. Although Chhabra et al. [5] identified a delay in chondrogenesis in the callus, they did not explore the mechanical integrity of the healed femur.

We therefore asked whether absence of GDF-5 during fracture repair impaired bone healing as assessed radiographically, histologically, and mechanically.

Materials and Methods

Using two independent groups, the contribution of GDF-5 to fracture healing was examined using a tibial osteotomy model. Ten-week-old male bp mice with a GDF-5 null mutation (A/J-GDF5 bp-J/+ bp; Jackson Laboratory, Bar Harbor, ME, USA) and their wild-type background counterparts (A/J; Jackson Laboratory) were compared over 56 days of healing (Fig. 1). The effect of GDF-5 function on repair was evaluated radiographically on Days 1, 10, 21, 28, and 56, by histologic profiling on Days 1 ($n = 1$ wild-type; $n = 5$ bp), 5 ($n = 3$ wild-type; $n = 3$ bp), 10 ($n = 6$ wild-type; $n = 3$ bp), 14 ($n = 6$ wild-type; $n = 6$ bp), 21 ($n = 6$ wild-type; $n = 6$ bp), 28 ($n = 7$ wild-type; $n = 6$ bp), and 56 ($n = 6$ wild-type; $n = 6$ bp) postfracture, through quantification of callus cross-sectional area on Days 10 ($n = 7$ wild-type; $n = 7$ bp contralateral and $n = 3$ bp fractured tibiae), 14 ($n = 6$ wild-type; $n = 6$ bp), 21 ($n = 6$ wild-type; $n = 6$ bp), 28 ($n = 6$ wild-type; $n = 3$ bp), and 56 ($n = 8$ wild-type; $n = 6$ bp) postfracture, and mechanically on Days 28 ($n = 6$ wild-type; $n = 3$ bp) and 56 ($n = 8$ wild-type; $n = 6$ bp) postfracture. All procedures involving animals were approved by the National Institutes of Health Animal Care and Use Committee.

We initially used a published model of murine tibial fracture in which the fracture is created by releasing a drop weight onto the bone stabilized with an intramedullary pin [22]; this model consistently resulted in shattering of the bp bones. Additionally, because bp mice have short tibiae with narrow marrow cavities (Fig. 2A–B), commonly used external fixators [4] also were inappropriate. It therefore was necessary to devise an alternative surgical technique. At 10 weeks of age, the animals were anesthetized with isoflurane (Fisher Scientific, Pittsburgh, PA, USA), and a longitudinal incision was created along the length of the lower right leg. Muscle and connective tissue on the medial side of the tibia were separated to expose the bone without disturbing the periosteum. Directly below the tuberosity of

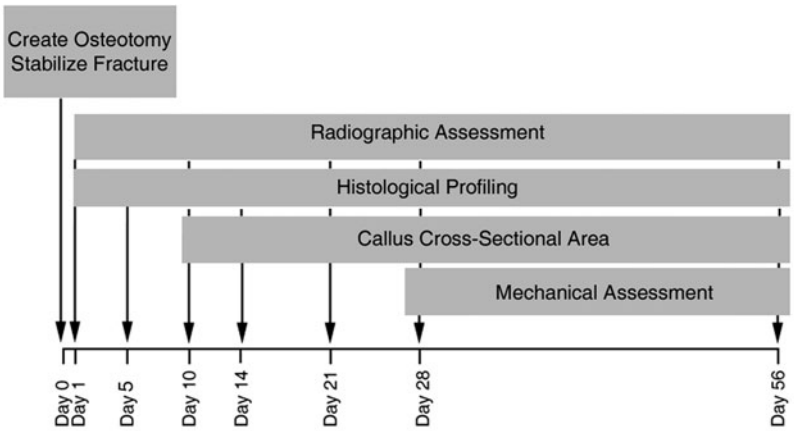

A

Day Postfracture	Histological Processing	Callus Cross-Sectional Area		Mechanical Assessment	
		Treated	Contralateral	Treated	Contralateral
Day 1 Control	n=1				
Day 1 bp	n=5				
Day 5 Control	n=3				
Day 5 bp	n=3				
Day 10 Control	n=6	n=7	n=7		
Day 10 bp	n=3	n=3	n=7		
Day 14 Control	n=6	n=6	n=6		
Day 14 bp	n=6	n=6	n=6		
Day 21 Control	n=6	n=6	n=6		
Day 21 bp	n=6	n=6	n=6		
Day 28 Control	n=7	n=6	n=6	n=6	n=6
Day 28 bp	n=6	n=3	n=3	n=3	n=3
Day 56 Control	n=6	n=8	n=8	n=8	n=8
Day 56 bp	n=6	n=6	n=3	n=3	n=3

B

Fig. 1A–B (**A**) Using two independent groups, the contribution of GDF-5 to fracture healing was assessed by a tibial osteotomy model stabilized by intramedullary and extramedullary fixation. Healing fractures in 10-week-old male bp mice with a GDF-5 null mutation and their wild-type background counterparts were compared during 56 days of healing. Radiographs were obtained of all animals participating in the study on Days 1, 10, 21, 28, and 56 after osteotomy. The effect of GDF-5 contribution to repair was assessed by histologic profiling on Days 1, 5, 10, 14, 21, 28, and 56 postfracture. Callus cross-sectional area was quantified on Days 10, 14, 21, 28, and 56 postfracture and mechanical assessments were conducted at Days 28 and 56 postfracture. (**B**) The number of biological replicates used for each outcome measure varied depending on time and assessment.

the tibia, a 0.5-mm hole was created using an ophthalmic burr creating an entry site for an intramedullary pin (Fig. 2C–D). A middiaphyseal osteotomy then was created with bone-cutting scissors and an intramedullary pin (000 gauge, 0.25 mm in diameter) inserted in the narrow marrow space (Fig. 2E–F). To prevent nonunions as a result of weightbearing-induced angulation of the intramedullary pin, a second 0-gauge pin was applied parallel to the medial surface of the tibia and anchored to the tibia with two resorbable sutures (Fig. 2G–H). Application of Nexaband (Abbott, North Chicago, IL, USA) surgical adhesive prevented the suture knots from loosening. The wound was closed with surgical staples, which were removed on postoperative Day 10. Animals were given 1.0 mg/kg buprenorphine every 8 to 12 hours for 2 days postoperatively and were permitted unrestricted weightbearing.

Radiographs were obtained using a Trophy IRIX 70 X-ray generator (Croissy Beaubourg, France) paired with an RVG digital sensor (Kodak, Atlanta, GA, USA) on the day of surgery, and again on Days 1, 10, 21, 28, and 56 after surgery.

For histologic evaluation, animals were euthanized after anesthesia by intracardiac injection of 4% paraformaldehyde (Sigma, St Louis, MO, USA). Both tibiae were dissected, rinsed in phosphate-buffered saline (Gibco, Carlsbad, CA, USA), and fixed in 4% paraformaldehyde. The samples were decalcified in 0.1 mol/L EDTA (Sigma), washed twice with diethylpyrocarbonate-treated water (Invitrogen, Carlsbad, CA, USA) dehydrated through a series of ethanol washes (Sigma), cleared with xylene (Sigma), and embedded in paraffin (Fisher Scientific). Eight-micrometer-thick sagittal sections were created using a Leica (Bannockburn, IL, USA) RM2165 microtome, placed on microscope slides, and stained with Safranin O and Fast Green (Sigma). An image of one slide per biological replicate was obtained using a Hamamatsu (Bridgewater, NJ, USA) Orca-ER digital camera mounted on a Leica DMRXE microscope on Days 1 ($n = 1$ wild-type; $n = 5$ bp), 5 ($n = 3$ wild-type; $n = 3$ bp), 10 ($n = 6$ wild-type; $n = 3$ bp), 14 ($n = 6$ wild-type; $n = 6$ bp), 21 ($n = 6$ wild-type; $n = 6$ bp), 28 ($n = 7$ wild-type; $n = 6$ bp), and 56 ($n = 6$ wild-type; $n = 6$ bp) postfracture. Using Openlab software (Perkin Elmer, Waltham, MA, USA), cartilage, organized bone, disorganized bone, and granular tissue were outlined by a reviewer based on histologic staining and tissue morphology. Openlab quantified the area of highlighted tissue from which the percent of the total area was calculated. Three reviewers

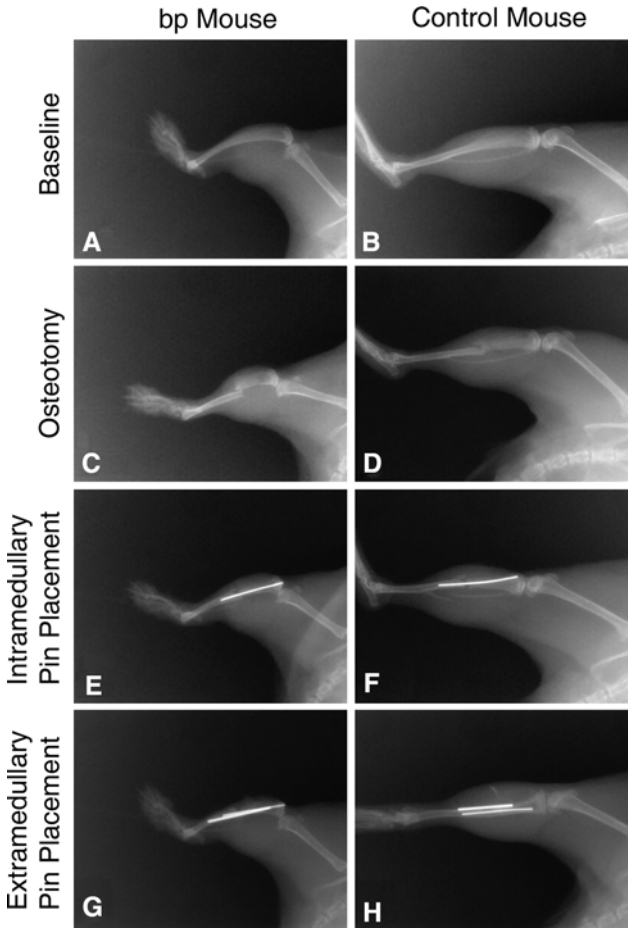

Fig. 2A–H Radiographs were obtained from bp and control wild-type mice throughout the fracturing and stabilization procedure, including presurgical baseline as seen in (**A**) the bp mouse and (**B**) control mouse; creation of the osteotomy as shown for the (**C**) bp mouse and (**D**) control mouse; placement of the intramedullary pins in the (**E**) bp mouse and (**F**) control mouse; and placement of extramedullary pins in the (**G**) bp mouse and (**H**) control mouse. There was a reduction in tibial length in (**A**) bp mice as compared with (**B**) control wild-type mice.

(EB, AB, BS) were trained to quantitatively evaluate the sections, and each section was handled by one of the reviewers.

Mechanical testing was conducted at Days 28 and 56 after fracturing. After dislocating the skull from the spinal column by applying manual pressure, both tibiae were explanted, rinsed, wrapped in phosphate-buffered saline-soaked gauze, and stored at −20°C. A custom four-point bending apparatus with a 10-pound load cell (Sensotec, Morristown, NJ, USA) was used to flex the thawed bones to failure (Fig. 3). The indenter spanned the fracture site (1.35 mm) and applied a constant rate of axial displacement (perpendicular to the long axis of the bone) at 1.5 μm per second (through an Oriel stepper motor and controller; Irvine, CA, USA) on either side of the callus until failure. Load and displacement were recorded simultaneously with

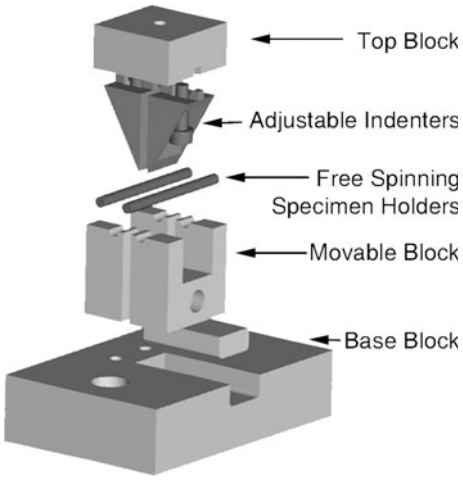

Fig. 3 To determine yield stress and Young's modulus, a custom four-point bending apparatus with a 10-pound load cell was designed to apply a constant rate of axial displacement until failure.

LabView software (National Instruments, Austin, TX, USA). The data are graphically displayed as the mean ± standard deviation.

After failure, a cross-sectional photograph of the fracture area was taken and converted into an eight-bit file with National Institutes of Health Image J (Bethesda, MD, USA) software. A custom program written in MATLAB (Natick, MA, USA) was used to determine the callus, cortical, and medullary cross-sectional areas of the fractured bones and to compute the bending moment of inertia (I). The modulus was calculated from the slope of the force-displacement curve (S) such that $E = SL^3/(48I)$. The ultimate strength (σult) was calculated from the peak force (Pmax) achieved with geometric considerations ($\sigma ult = PmaxLD/8I$).

Statistical analysis of histologic scoring evaluating differences in tissue composition between bp and control fractures was evaluated with Student's T-test using a two-tailed distribution with equal variance on Microsoft Excel (Chevy Chase, MD, USA). Statistical evaluation of callus cross-sectional area, yield stress, and modulus between contralateral control and fractured conditions for bp and background wild-type control groups was conducted using one-way ANOVA with a Tukey's post hoc test using Microsoft Excel.

Results

Radiographic profiling of fracture repair indicated a similar rate of callus formation and ossification in bp and wild-type control mice. Initially, no callus was observed in either group (Fig. 4A–B); however, after 10 days, a callus had formed only in control animals (Fig. 4C–D). Control and bp fracture sites were denser at 21 days, suggesting

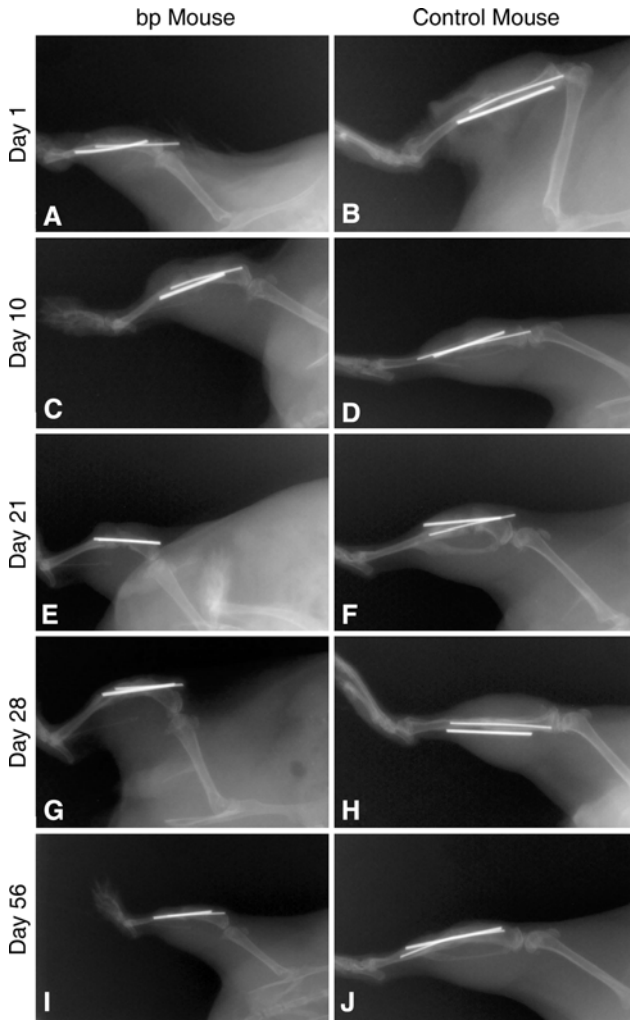

Fig. 4A–J Radiographs were acquired at Day 1 for (**A**) bp and (**B**) control wild-type mice; Day 10 for (**C**) bp and (**D**) control wild-type mice; Day 21 for (**E**) bp and (**F**) control wild-type mice; Day 28 for (**G**) bp and (**H**) control wild-type mice; and Day 56 for (**I**) bp and (**J**) control wild-type mice for evidence of healing postfracture. The creation of the (**A–B**) fracture, (**C–F**) callus formation, and (**G–J**) bone remodeling were observed.

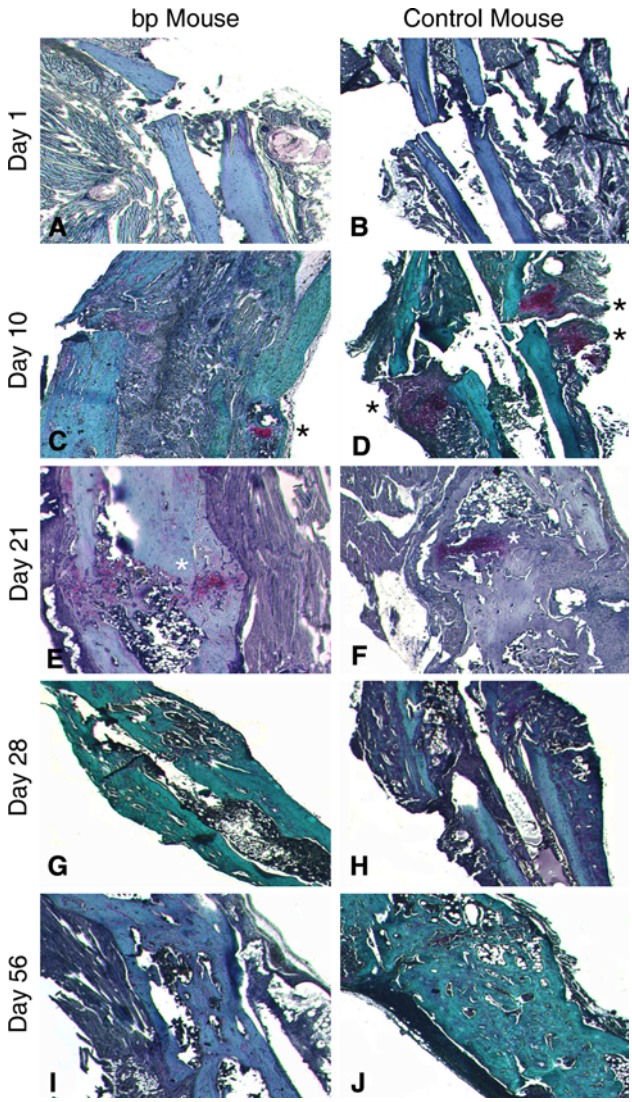

Fig. 5A–J Tibiae were isolated from bp and control wild-type mice, embedded, sectioned, and stained with Safranin O and Fast Green at Day 1 for (**A**) bp and (**B**) control wild-type mice; Day 10 for (**C**) bp and (**D**) control wild-type mice; Day 21 for (**E**) bp and (**F**) control wild-type mice; Day 28 for (**G**) bp and (**H**) control wild-type mice; and Day 56 for (**I**) bp and (**J**) control wild-type mice of healing postfracture. Blue or green staining indicates bone, pink staining denotes cartilaginous tissue or sutures, and purple staining indicates granular tissue. To highlight the presence of cartilage, it has been marked with a black or white asterisk. The (**A–B**) initial morphologic features of the fractures were similar in bp and control animals, but by Day 10, there was an increase in cellularity in (**C**) bp mice as compared with (**D**) controls. The wild-type callus contains cartilaginous deposits, whereas the bp callus does not. At Day 21 postosteotomy, cartilage formation was evident in (**E**) bp mice, whereas the (**F**) control fractures were undergoing remodeling of the cartilaginous precursor into bone. At (**G–H**) Days 28 and (**I–J**) 56 postfracture, the fracture was calcified, but remodeling of the callus was incomplete (Stain, Safranin O and Fast Green counterstained, original magnification, ×10).

calcification (Fig. 4E–F) and remodeling by Day 28 as indicated by reduced callus size (Fig. 4G–H). Fifty-six days postfracture, the callus in both groups remodeled to their native shape (Fig. 4I–J); however, the fractured tibiae were denser than in nonfractured contralateral control bones, suggesting remodeling was not complete.

Immediately after surgery, there were no noticeable histologic differences between the study groups (Fig. 5A–B). By Day 10, control calluses contained dramatically more cartilage, while bp fracture calluses retained granular tissue (Fig. 5C–D). After 21 days, cartilage formation was evident in bp fractures (Fig. 5E), while the control fractures showed evidence of remodeling into bone (Fig. 5F). At Days 28 (Fig. 5G–H) and 56 (Fig. 5I–J) postfracture, the fracture was calcified, but its remodeling remained incomplete. Histologic evaluation of repair tissue composition in bp and wild-type control mice showed a decrease

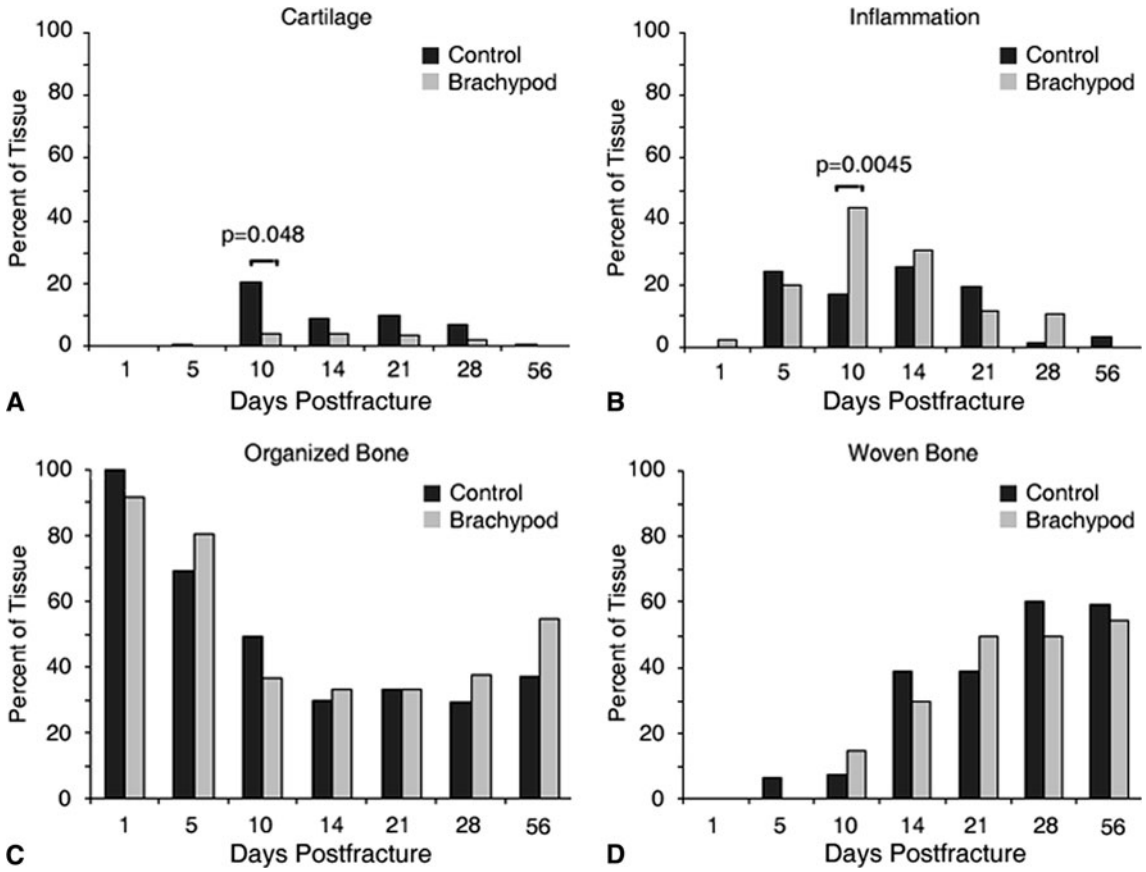

Fig. 6A–D The composition of the cartilaginous, inflammatory, and ossified callus was analyzed as a function of postfracture time in bp (gray) and control (black) treatment groups by morphometry. The temporal profile of cartilage deposition was similar in both treatment groups, peaking at (**A**) Day 10; however, substantially more cartilage was present in control calluses as compared with bp calluses at Days 10 through 21. The temporal profile of (**B**) inflammatory cell infiltration in the callus was similar in bp and control mice, peaking at Day 10 with greater amounts of inflammatory infiltration in bp fractures. There was a steep initial decrease in (**C**) organized bone in bp and control mice and increase in (**D**) woven bone after fracturing, with a plateau reached between Days 10 and 20 postfracture. Although the final amount of bone deposited was similar, there was more woven bone present in control animals at an earlier time as compared with bp mice.

in cartilage deposition in the absence of GDF-5, particularly at Days 10 and 21. The deposition of cartilage proceeded in a similar temporal profile in bp and control animals (Fig. 6A), however, the amount of cartilage in bp animals was substantially less than in controls at Day 10. Both study groups had a similar temporal profile of inflammatory cell infiltration, starting immediately after injury, peaking at Day 10, and decreasing thereafter. However, the bp fracture contained substantially more cellularity (Fig. 6B), which was maintained at the fracture side after control levels returned to baseline. Woven and organized bone were similarly deposited, temporally and in quantity, in both groups (Fig. 6C–D) in which a steep initial decrease in organized bone and increase in woven bone after fracture were observed, stabilizing between 10 and 20 days postfracture. Although the final amount of bone deposited was similar, there was more woven bone present in control animals at an earlier time as compared with bp mice.

We observed reduced callus cross-sectional area in bp mice; however the repaired fracture was mechanically similar in the absence of GDF-5. Although the nonfractured tibial cross-sectional areas were similar in both groups, the bp calluses were consistently smaller than the control calluses (Fig. 7). With time, bp callus areas were equivalent to those of their nonfractured contralateral controls, whereas the wild-type calluses remained substantially larger than those of nonfractured controls. We observed a decrease in yield stress at Days 28 ($p = 0.0005$ in wild-type controls and $p = 0.0001$ in bp animals) and 56 ($p = 0.0130$ in wild-type controls and $p = 0.0428$ in bp animals) in fractured tibiae as compared with nonfractured contralateral controls (Fig. 8). We similarly observed a decrease ($p = 0.004$) in Young's modus in fractured bp tibiae as compared with contralateral controls. Although the mechanical integrity of nonfractured contralateral controls increased as the mice aged, the relative values between the fractured and

nonfractured contralateral tibiae were similar in the bp and wild-type animals.

Discussion

GDF-5 is a key regulator of embryonic skeletal development as evidenced by its specific expression in precartilage condensations [7, 15, 43], on articular surfaces and joint interzones, and along the perichondrium [7, 15]. De novo bone formation can be stimulated in vivo by ectopic application of GDF-5 for spinal fusion [26, 39, 40] and nonunion fracture repair [39, 40] indicating the potential of GDF-5 in orthopaedic applications. The functional roles of GDF-5 in bone fracture repair involve enhancement of osteogenic differentiation [38, 49, 51, 52] and the stimulation of angiogenesis [37]. We therefore asked whether absence of GDF-5 during fracture repair impaired bone healing as assessed radiographically, histologically, and mechanically.

There are several limitations to this study. First, we had no quantitative method, such as blinded evaluation of radiographs or microCT, to evaluate bone mineral density. Although detailed evaluation of mineral density would enhance this investigation, we do not base the interpretation of this study on bone density and therefore consider such analysis to be supplementary and not critical in the study. Second, we did not explore the role of GDF-5 in the healing of nonunion fractures, as this was investigated by Spiro et al. [39, 40]. Third, the formation of intramedullary bone as a result of fracture fixation, a variable that may impair endochondral ossification, was not investigated.

The method of fracture fixation used here could significantly influence the process of fracture repair. As this fracture was created by osteotomy to avoid damage to the periosteum along with application of a stabilizing fixative at the suture points, the ends of the long bone were set in close proximity. A stable fracture fixation method such as this may support anastomosis at the end of long bone segments, leading to intramembranous bone healing [23]. Together, these factors may support intramembranous bone

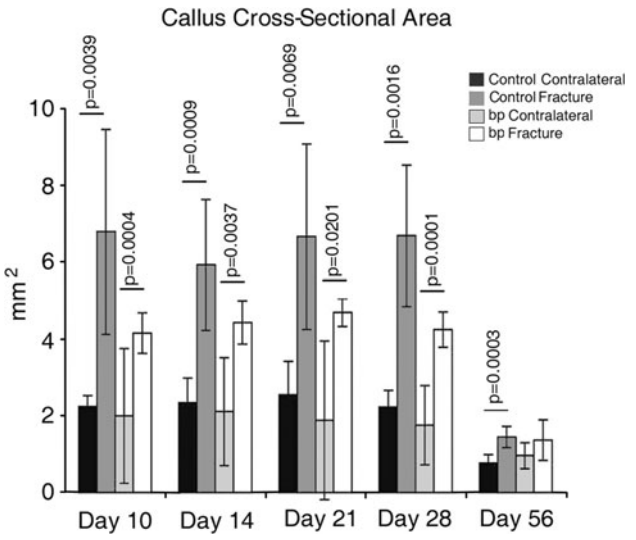

Fig. 7 The cross-sectional area of calluses at the site of failure were determined using image analysis software after mechanical testing in control wild-type (dark) and bp (light) fractured and nonfractured contralateral controls. The cross-sectional area was consistently greater in fractured bones as compared with nonfractured contralateral controls at all times with the exception of bp samples at Day 56. Control fracture calluses were consistently larger than bp fracture calluses at Days 10, 14, 21, and 28.

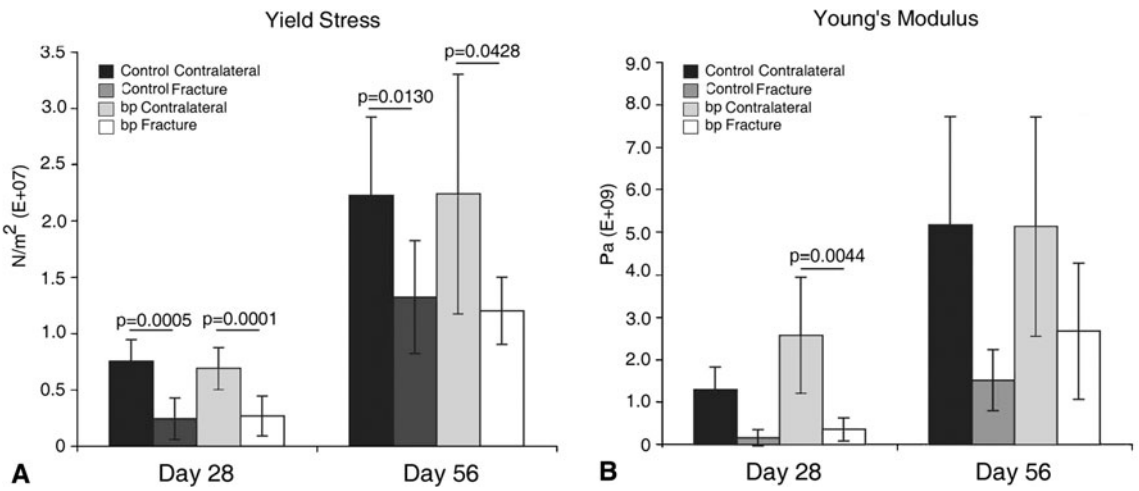

Fig. 8A–B (**A**) Yield stress and (**B**) Young's modulus measurements in control (dark) and bp (light) fractured and nonfractured contralateral tibiae at 28 and 56 days postfracture showed that the control and bp fractured tibiae were weaker than their respective nonfractured contralateral controls. No difference was observed in yield stress between bp and wild-type fractured calluses. With time, the baseline yield stress and Young's modulus increased in bp and wild-type groups, suggesting a stiffer bone with age.

formation in parallel to endochondral ossification. However, in this study the histologic and radiographic endpoints focused solely on measures of endochondral ossification and not intramembranous, leaving an opportunity for future investigations.

We analyzed the fractured bp tibiae histologically to assess cellular infiltration and the extent of chondrogenesis and ossification. Control mice had a histologically normal healing profile [22], thus validating the modified fracture protocol we developed. At Day 10 postfracture, bp mice showed substantial infiltration of inflammatory cells and an absence of cartilage formation as compared with control mice. This delay in chondrogenesis continued through the first 3 weeks of healing, after which the fracture morphology was comparable in both groups. These data are similar to those profiled previously indicating enhanced cellular infiltration and delayed chondrogenesis in bp fracture repair [5]. Because healing was temporally similar in bp and control mice, it is likely the stimulatory signals initiating general cellular infiltration and callus formation were released in the appropriate spatiotemporal profile in bp mice and that the responding cells were present and capable. However, the specific reduction in cartilage quantity would suggest a particular inadequacy in the initiation of chondrogenesis in the fractured bp tibiae, as would be expected in a tissue environment deficient in GDF-5. Because GDF-5 deficiency causes alterations in cell migration [15, 21], cell condensation [8], chondrogenesis [8, 15], and chondrocyte hypertrophy [9], it therefore is consistent that bp callus areas were reduced in size with minimal cartilage formation.

Image analysis of the histologic specimens showed the bp callus contained substantially more inflammatory tissue for a longer time but peaking similarly to controls at Day 10 postfracture. Although the presence of inflammatory cells diminished with time, it was not replaced with cartilage as in control animals. Because cartilage formation in the soft callus of bp mice was reduced and delayed, the corresponding increase in inflammatory tissue possibly impaired the mechanical stability normally provided by cartilage. The composition of the hard callus was comparable in terms of the temporal profile of formation and in quantity between the control and bp animals.

Cross-sectional area analysis and mechanical testing showed comparable structural integrity in the healing fractures between the control and bp animals in the late stage of fracture healing. These data differ from those reported previously [5], in which a delay in bp fractures reaching peak callus area was observed. However, in this study after 56 days, the remodeled bp callus area was similar to that in the nonfractured contralateral control. The strength of repairing bp fractures was consistently comparable to that of the wild-type controls. After 56 days, we observed a trend for greater stiffness in repairing bp fractures. The mechanical integrity data of the nonfractured control tibiae presented here differ from those reported by Mikic et al. in which bp femurs were mechanically inferior to those of wild-type controls [32]. This disagreement may be the result of using a different testing method (bending versus torque) to measure mechanical stability, the inherent difference between the tibial or femoral mechanics, or the skeletal maturity of the mice used in the model system.

Because GDF-5 deficiency causes alterations in cell migration [15, 21], cell condensation [8], chondrogenesis [8, 15], and chondrocyte hypertrophy [9], it therefore is consistent that bp fractures were reduced in size with delayed and reduced chondrogenesis. As fracture repair recapitulates many aspects of embryonic skeletal development, it can be extrapolated that GDF-5 in the callus acts to stimulate reparative cell recruitment, condensation, and chondrogenic differentiation, and possibly also initiate vascularization. The lack of functional GDF-5 in bp mice thus might result specifically in a decrease in progenitor cell recruitment from the marrow stroma and/or periosteum. Reduced progenitor cell number and/or density, along with the absence of GDF-5-stimulated chondrogenic signaling, therefore would lead to decreased cellular condensation and chondrogenesis, resulting in reduced callus cross-sectional area and cartilage composition. Given its proangiogenic activity, the absence of GDF-5 also might result in decreased vascularization and therefore delayed transition from callus to bone [48]. Alternatively, delayed chondrogenesis and subsequent bone remodeling as a result of GDF-5 deficiency may have been compensated for by other factors, such as intramembranous bone formation.

GDF-5 deficiency impairs the chondrogenic process during fracture healing, although ultimately the bones heal as well as in control mice. Because GDF-5 is a potent activator of chondrogenesis in callus formation, and therefore a key moderator of fracture healing, the application of GDF-5 as a therapeutic factor for nonunion fracture healing is of considerable interest for further investigation.

Acknowledgment We thank Erika Bickler for her technical contribution to this work.

References

1. Al-Yahyaee SA, Al-Kindi MN, Habbal O, Kumar DS. Clinical and molecular analysis of Grebe acromesomelic dysplasia in an Omani family. *Am J Med Genet A.* 2003;121A:9–14.
2. Bai X, Xiao Z, Pan Y, Hu J, Pohl J, Wen J, Li L. Cartilage-derived morphogenetic protein-1 promotes the differentiation of mesenchymal stem cells into chondrocytes. *Biochem Biophys Res Commun.* 2004;325:453–460.

3. Chang SC, Hoang B, Thomas JT, Vukicevic S, Luyten FP, Ryba NJ, Kozak CA, Reddi AH, Moos M Jr. Cartilage-derived morphogenetic proteins: new members of the transforming growth factor-beta superfamily predominantly expressed in long bones during human embryonic development. *J Biol Chem.* 1994;269: 28227–28234.
4. Cheung KM, Kaluarachi K, Andrew G, Lu W, Chan D, Cheah KS. An externally fixed femoral fracture model for mice. *J Orthop Res.* 2003;21:685–690.
5. Chhabra A, Zijerdi D, Zhang J, Kline A, Balian G, Hurwitz S. BMP-14 deficiency inhibits long bone fracture healing: a biochemical, histologic, and radiographic assessment. *J Orthop Trauma.* 2005;19:629–634.
6. Cho TJ, Gerstenfeld LC, Einhorn TA. Differential temporal expression of members of the transforming growth factor beta superfamily during murine fracture healing. *J Bone Miner Res.* 2002;17:513–520.
7. Coleman CM, Loredo GA, Lo CW, Tuan RS. Correlation of GDF5 and connexin 43 mRNA expression during embryonic development. *Anat Rec A Discov Mol Cell Evol Biol.* 2003;275: 1117–1121.
8. Coleman CM, Tuan RS. Functional role of growth/differentiation factor 5 in chondrogenesis of limb mesenchymal cells. *Mech Dev.* 2003;120:823–836.
9. Coleman CM, Tuan RS. Growth/differentiation factor 5 enhances chondrocyte maturation. *Dev Dyn.* 2003;228:208–216.
10. Costa T, Ramsby G, Cassia F, Peters KR, Soares J, Correa J, Quelce-Salgado A, Tsipouras P. Grebe syndrome: clinical and radiographic findings in affected individuals and heterozygous carriers. *Am J Med Genet.* 1998;75:523–529.
11. Erlacher L, McCartney J, Piek E, ten Dijke P, Yanagishita M, Oppermann H, Luyten FP. Cartilage-derived morphogenetic proteins and osteogenic protein-1 differentially regulate osteogenesis. *J Bone Miner Res.* 1998;13:383–392.
12. Everman DB, Bartels CF, Yang Y, Yanamandra N, Goodman FR, Mendoza-Londono JR, Savarirayan R, White SM, Graham JM Jr, Gale RP, Svarch E, Newman WG, Kleckers AR, Francomano CA, Govindaiah V, Singh L, Morrison S, Thomas JT, Warman ML. The mutational spectrum of brachydactyly type C. *Am J Med Genet.* 2002;112:291–296.
13. Faiyaz-Ul-Haque M, Ahmad W, Wahab A, Haque S, Azim AC, Zaidi SH, Teebi AS, Ahmad M, Cohn DH, Siddique T, Tsui LC. Frameshift mutation in the cartilage-derived morphogenetic protein 1 (CDMP1) gene and severe acromesomelic chondrodysplasia resembling Grebe-type chondrodysplasia. *Am J Med Genet.* 2002;111:31–37.
14. Faiyaz-Ul-Haque M, Ahmad W, Zaidi SH, Haque S, Teebi AS, Ahmad M, Cohn DH, Tsui LC. Mutation in the cartilage-derived morphogenetic protein-1 (CDMP1) gene in a kindred affected with fibular hypoplasia and complex brachydactyly (DuPan syndrome). *Clin Genet.* 2002;61:454–458.
15. Francis-West PH, Abdelfattah A, Chen P, Allen C, Parish J, Ladher R, Allen S, MacPherson S, Luyten FP, Archer CW. Mechanisms of GDF-5 action during skeletal development. *Development.* 1999;126:1305–1315.
16. Galjaard RJ, van der Ham LI, Posch NA, Dijkstra PF, Oostra BA, Hovius SE, Timmenga EJ, Sonneveld GJ, Hoogeboom AJ, Heutink P. Differences in complexity of isolated brachydactyly type C cannot be attributed to locus heterogeneity alone. *Am J Med Genet.* 2001;98:256–262.
17. Gerstenfeld LC, Cullinane DM, Barnes GL, Graves DT, Einhorn TA. Fracture healing as a post-natal developmental process: molecular, spatial, and temporal aspects of its regulation. *J Cell Biochem.* 2003;88:873–884.
18. Gruber R, Mayer C, Bobacz K, Krauth MT, Graninger W, Luyten FP, Erlacher L. Effects of cartilage-derived morphogenetic proteins and osteogenic protein-1 on osteochondrogenic differentiation of periosteum-derived cells. *Endocrinology.* 2001;142: 2087–2094.
19. Gruber R, Mayer C, Schulz W, Graninger W, Peterlik M, Watzek G, Luyten FP, Erlacher L. Stimulatory effects of cartilage-derived morphogenetic proteins 1 and 2 on osteogenic differentiation of bone marrow stromal cells. *Cytokine.* 2000;12: 1630–1638.
20. Gruneberg H, Lee AJ. The anatomy and development of brachypodism in the mouse. *J Embryol Exp Morphol.* 1973;30: 119–141.
21. Hatakeyama Y, Tuan RS, Shum L. Distinct functions of BMP4 and GDF5 in the regulation of chondrogenesis. *J Cell Biochem.* 2004;91:1204–1217.
22. Hiltunen A, Vuorio E, Aro HT. A standardized experimental fracture in the mouse tibia. *J Orthop Res.* 1993;11:305–312.
23. Histing T, Garcia P, Matthys R, Leidinger M, Holstein JH, Kristen A, Pohlemann T, Menger MD. An internal locking plate to study intramembranous bone healing in a mouse femur fracture model. *J Orthop Res.* 2010;28:397–402.
24. Holder-Espinasse M, Escande F, Mayrargue E, Dieux-Coeslier A, Fron D, Doual-Bisser A, Boute-Benejean O, Robert Y, Porchet N, Manouvrier-Hanu S. Angel shaped phalangeal dysplasia, hip dysplasia, and positional teeth abnormalities are part of the brachydactyly C spectrum associated with CDMP-1 mutations. *J Med Genet.* 2004;41:e78.
25. Hotten G, Neidhardt H, Jacobowsky B, Pohl J. Cloning and expression of recombinant human growth/differentiation factor 5. *Biochem Biophys Res Commun.* 1994;204:646–652.
26. Jahng TA, Fu TS, Cunningham BW, Dmitriev AE, Kim DH. Endoscopic instrumented posterolateral lumbar fusion with Healos and recombinant human growth/differentiation factor-5. *Neurosurgery.* 2004;54:171–180; discussion 180–181.
27. Kjaer KW, Eiberg H, Hansen L, van der Hagen CB, Rosendahl K, Tommerup N, Mundlos S. A mutation in the receptor binding site of GDF5 causes Mohr-Wriedt brachydactyly type A2. *J Med Genet.* 2006;43:225–231.
28. Koch H, Jadlowiec JA, Fu FH, Nonn J, Merk HR, Hollinger JO, Campbell PG. [The effect of growth/differentiation factor-5 (GDF-5) on genotype and phenotype in human adult mesenchymal stem cells] [in German]. *Z Orthop Ihre Grenzgeb.* 2004;142: 248–253.
29. Kuniyasu H, Hirose Y, Ochi M, Yajima A, Sakaguchi K, Murata M, Pohl J. Bone augmentation using rhGDF-5-collagen composite. *Clin Oral Implants Res.* 2003;14:490–499.
30. Landauer W. Brachypodism: a recessive mutation of house-mice. *J Hered.* 1952;43:724–732.
31. Lin K, Thomas JT, McBride OW, Luyten FP. Assignment of a new TGF-beta superfamily member, human cartilage-derived morphogenetic protein-1, to chromosome 20q11.2. *Genomics.* 1996;34:150–151.
32. Mikic B, Battaglia TC, Taylor EA, Clark RT. The effect of growth/differentiation factor-5 deficiency on femoral composition and mechanical behavior in mice. *Bone.* 2002;30:733–737.
33. Polinkovsky A, Robin NH, Thomas JT, Irons M, Lynn A, Goodman FR, Reardon W, Kant SG, Brunner HG, van der Burgt I, Chitayat D, McGaughran J, Donnai D, Luyten FP, Warman ML. Mutations in CDMP1 cause autosomal dominant brachydactyly type C. *Nat Genet.* 1997;17:18–19.
34. Sato M, Ochi T, Nakase T, Hirota S, Kitamura Y, Nomura S, Yasui N. Mechanical tension-stress induces expression of bone morphogenetic protein (BMP)-2 and BMP-4, but not BMP-6, BMP-7, and GDF-5 mRNA, during distraction osteogenesis. *J Bone Miner Res.* 1999;14:1084–1095.
35. Schwabe GC, Turkmen S, Leschik G, Palanduz S, Stover B, Goecke TO, Mundlos S. Brachydactyly type C caused by a

homozygous missense mutation in the prodomain of CDMP1. *Am J Med Genet A.* 2004;124A:356–363.
36. Seemann P, Schwappacher R, Kjaer KW, Krakow D, Lehmann K, Dawson K, Stricker S, Pohl J, Ploger F, Staub E, Nickel J, Sebald W, Knaus P, Mundlos S. Activating and deactivating mutations in the receptor interaction site of GDF5 cause symphalangism or brachydactyly type A2. *J Clin Invest.* 2005;115: 2373–2381.
37. Sena K, Sumner DR, Virdi AS. Modulation of VEGF expression in rat bone marrow stromal cells by GDF-5. *Connect Tissue Res.* 2007;48:324–331.
38. Shen FH, Zeng Q, Lv Q, Choi L, Balian G, Li X, Laurencin CT. Osteogenic differentiation of adipose-derived stromal cells treated with GDF-5 cultured on a novel three-dimensional sintered microsphere matrix. *Spine J.* 2006;6:615–623.
39. Spiro RC, Liu L, Heidaran MA, Thompson AY, Ng CK, Pohl J, Poser JW. Inductive activity of recombinant human growth and differentiation factor-5. *Biochem Soc Trans.* 2000;28:362–368.
40. Spiro RC, Thompson AY, Poser JW. Spinal fusion with recombinant human growth and differentiation factor-5 combined with a mineralized collagen matrix. *Anat Rec.* 2001;263:388–395.
41. Stelzer C, Winterpacht A, Spranger J, Zabel B. Grebe dysplasia and the spectrum of CDMP1 mutations. *Pediatr Pathol Mol Med.* 2003;22:77–85.
42. Storm EE, Huynh TV, Copeland NG, Jenkins NA, Kingsley DM, Lee SJ. Limb alterations in brachypodism mice due to mutations in a new member of the TGF beta-superfamily. *Nature.* 1994;368: 639–643.
43. Storm EE, Kingsley DM. GDF5 coordinates bone and joint formation during digit development. *Dev Biol.* 1999;209:11–27.
44. Szczaluba K, Hilbert K, Obersztyn E, Zabel B, Mazurczak T, Kozlowski K. Du Pan syndrome phenotype caused by heterozygous pathogenic mutations in CDMP1 gene. *Am J Med Genet A.* 2005;138:379–383.
45. Thomas JT, Kilpatrick MW, Lin K, Erlacher L, Lembessis P, Costa T, Tsipouras P, Luyten FP. Disruption of human limb morphogenesis by a dominant negative mutation in CDMP1. *Nat Genet.* 1997;17:58–64.
46. Tsumaki N, Tanaka K, Arikawa-Hirasawa E, Nakase T, Kimura T, Thomas JT, Ochi T, Luyten FP, Yamada Y. Role of CDMP-1 in skeletal morphogenesis: promotion of mesenchymal cell recruitment and chondrocyte differentiation. *J Cell Biol.* 1999; 144:161–173.
47. Wolfman NM, Hattersley G, Cox K, Celeste AJ, Nelson R, Yamaji N, Dube JL, DiBlasio-Smith E, Nove J, Song JJ, Wozney JM, Rosen V. Ectopic induction of tendon and ligament in rats by growth and differentiation factors 5, 6, and 7, members of the TGF-beta gene family. *J Clin Invest.* 1997;100:321–330.
48. Yamashita H, Shimizu A, Kato M, Nishitoh H, Ichijo H, Hanyu A, Morita I, Kimura M, Makishima F, Miyazono K. Growth/differentiation factor-5 induces angiogenesis in vivo. *Exp Cell Res.* 1997;235:218–226.
49. Yeh LC, Tsai AD, Lee JC. Cartilage-derived morphogenetic proteins induce osteogenic gene expression in the C2C12 mesenchymal cell line. *J Cell Biochem.* 2005;95:173–188.
50. Yoshimoto T, Yamamoto M, Kadomatsu H, Sakoda K, Yonamine Y, Izumi Y. Recombinant human growth/differentiation factor-5 (rhGDF-5) induced bone formation in murine calvariae. *J Periodontal Res.* 2006;41:140–147.
51. Zeng Q, Li X, Beck G, Balian G, Shen FH. Growth and differentiation factor-5 (GDF-5) stimulates osteogenic differentiation and increases vascular endothelial growth factor (VEGF) levels in fat-derived stromal cells in vitro. *Bone.* 2007;40:374–381.
52. Zeng Q, Li X, Choi L, Beck G, Balian G, Shen FH. Recombinant growth/differentiation factor-5 stimulates osteogenic differentiation of fat-derived stromal cells in vitro. *Connect Tissue Res.* 2006;47:264–270.